Methyl Iodide Oxidative Addition to Rhodium(I) Complexes: a DFT and NMR Study of [Rh(FcCOCHCOCF$_3$)(CO)(PPh$_3$)] and the Rhodium(III) Reaction Products

Marrigje M. Conradie and Jeanet Conradie*

Department of Chemistry, University of the Free State, Bloemfontein, 9301 South Africa

Received 8 February 2008, revised 18 June 2008, accepted 12 September 2008.

ABSTRACT

A theoretical (DFT) study of the equilibrium geometry of the possible reaction products of the oxidative addition reaction [Rh(FcCOCHCOCF$_3$)(CO)(PPh$_3$)] + CH$_3$I (Fc = ferrocenyl), consistent with experimental observations, revealed that the first alkyl product results from *trans* addition to Rh^I. Isomerization *via* an acyl intermediate leads to a second octahedral alkyl product with the PPh$_3$ group and the iodide above and below the square plane. Theoretical computations also revealed that the thermodynamic acyl product adopts a square-pyramidal geometry with the COCH$_3$ group in the apical position.

KEYWORDS

DFT, computational, rhodium, β-diketone, NMR.

1. Introduction

The chemistry of rhodium is very important for catalytic applications since the metal can easily coordinate with many organic and inorganic molecules, which are in turn very reactive and widely used for fundamental investigations on catalysis in both the laboratory and in industry. A classic example of an efficacious catalyst system is the methanol carbonylation to acetic acid in the presence of $[Rh(CO)_2I_2]^-$. Methanol carbonylation with the original Monsanto catalyst has been studied in detail, not only experimentally,[1–7] but also from a theoretical point of view.[6,8–10] In contrast, the same reaction promoted from rhodium(I) carbonyl phosphine complexes has been the subject of detailed experimental research,[11–18] but not from a theoretical point of view. This is despite the potential of computational chemistry to contribute to the understanding of the role of the steric and electronic properties of the different ligands to determine the relative rates of the two most important steps of the catalytic cycle, i.e. the oxidative addition and the CO migratory insertion steps resulting in Rh^{III}-alkyl and Rh^{III}-acyl products.

Oxidative addition reactions of square planar Rh(I) complexes proceed via different reaction pathways and the addition can be either *cis* or *trans*. It is therefore important to know the molecular structures of the reactants and products, as well as the nature of the intermediates, to propose suitable reaction mechanisms. Based on experimental kinetic studies,[13,14,19,20] the proposed mechanism of the oxidative addition of CH$_3$I to Rh(I) carbonyl phosphine complexes is a nucleophilic attack by the rhodium atom on the carbon atom of the methyl iodide, where a linear polar transition state is formed which leads to *trans* addition (see Fig. 1), although the possibility of a three-centred polar transition state, which normally leads to *cis* addition, cannot be ruled out.[21] Although the first reaction product of the square planar Rh(I) carbonyl phosphine complexes with methyl iodide is a Rh^{III}-alkyl species, mechanistic concepts suggest in many cases that the oxidative addition reaction proceeds through Rh^{III}-alkyl and Rh^{III}-acyl intermediates. The final or most stable reaction products that form are octahedral or square-pyramidal complexes of rhodium(III) with different mutual disposition of the ligands.[17,22–30]

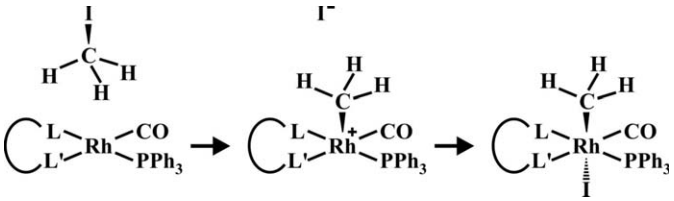

Figure 1 S_N2 mechanism for the oxidative addition of CH$_3$I to a square planar Rh^I carbonyl phosphine complex containing a monoanionic bidentate β-diketonato ligand.

On the basis of extensive kinetic studies of these reactions, the mechanistic schemes proposed for the oxidative addition of methyl iodide to [Rh^I(L,L′-BID)(CO)(PPh$_3$)], where L,L′-BID is a monoanionic bidentate ligand with donor atoms L and L′ or β-diketonato complexes, can be summarized as in Scheme 1:[31]

[Rh^I(L,L'-BID)(CO)(PPh$_3$)] isomers + CH$_3$I

k_{-1} ⇌ k_1

Rh^{III}-alkyl1 isomers

k_{-2} ⇌ k_2

Rh^{III}-acyl1 isomers

k_{-3} ⇌ k_3

Rh^{III}-alkyl2 isomers

k_{-4} ⇌ k_4

Rh^{III}-acyl2 isomers

Scheme 1

*To whom correspondence should be addressed. E-mail: conradj.sci@ufs.ac.za

For [Rh^{I}(L,L′-BID)(CO)(PPh$_3$)] complexes containing an unsymmetrical bidentate ligand L,L′-BID, generally at least two structural isomers for rhodium(I) as well as for each rhodium(III) reaction intermediate (according to Scheme 1) are observed by NMR spectroscopy.[32] The notation Rh^{III}-alkyl1 and Rh^{III}-acyl1 in the above scheme indicates the first formed alkylated [Rh^{III}(L,L′-BID)(CH$_3$)(CO)(PPh$_3$)(I)] or acylated [Rh^{III}(L,L′-BID)(COCH$_3$)(PPh$_3$)(I)] species. When the last number in the notation changes to 2, such as in Rh^{III}-alkyl2, it shows that after the first alkylated or acylated species has formed, it converted to a second, different but more stable, alkylated or acylated structural isomer.

Characterization of the Rh^{III} reaction products according to Scheme 1 includes:

1. distinction between Rh^{III}-alkyl and Rh^{III}-acyl products by IR spectroscopy,[11–17]
2. a NMR spectral study of the products formed by the reaction between [Rh^{I}(L,L′-BID)(CO)(PPh$_3$)] and methyl iodide[31–34] and
3. crystal structure determination of selected products.[17,22–30,32]

Several crystal structures[35] of the products of the oxidative addition of methyl iodide to [Rh^{I}(L,L′-BID)(CO)(PPh$_3$)] are available. However, except for one ferrocenyl-containing Rh^{III}-alkyl2 structure,[32] it is not known at which stage of the reaction according to Scheme 1 the crystals were isolated, i.e. it is not known if the crystals represent an alkyl1, alkyl2, acyl1 or acyl2 species. The available crystal structures can be conveniently combined into three classes (see Fig. 2).

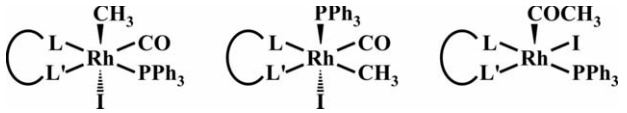

Figure 2 The three classes of geometrical structures from crystal structure determination of isolated products of the oxidative addition of methyl iodide to [Rh^{III}(L,L′–BID)(CO)(PPh$_3$)], where L,L′-BID = monoanionic bidentate ligand with donor atoms L and L′: Class 1 – CH$_3$ and I *trans,* Class 2 – CH$_3$ and I *cis,* and Class 3 – COCH$_3$ in apical position.

Class 1: Rh^{III}-alkyl products where the methyl and the iodide are above and below the square plane (L,L′-BID = ox (Hox = 8-hydroxyquinoline),[22] (PhCOCHPPh$_2$)$^-$,[23] dmavk (Hdmavk = dimethylaminovinylketone)[24]).

Class 2: Rh^{III}-alkyl products where the PPh$_3$ and the iodide are above and below the square plane (L,L′-BID = cupf (Hcupf = N-hydroxy-N-nitroso-benzeneamine),[25] (OCO(C$_9$H$_6$N))$^-$,[26] neocupf (Hneocupf = N-nitroso-N-naphthylhydroxylamine),[27] fctfa (Hfctfa = 1-ferrocenyl-4,4,4-trifluorobutane-1,3-dione)[32]).

Class 3: Rh^{III}-acyl products where the acyl moiety is in the apical position (L,L′-BID = (PhCOCHPPh$_2$)$^-$,[28] mnt (Hmnt = maleonitriledithiolate),[29] dmavk,[30] and stsc (Hstsc = salicylaldehydethiosemicarbazone).[17]

The specific stereochemistry of the different rhodium(III) reaction products Rh^{III}-alkyl1, Rh^{III}-alkyl2, Rh^{III}-acyl1 and Rh^{III}-acyl2 in the course of the reaction, as given by Scheme 1, is thus unknown, except for the crystal structure of [Rh^{III}(fctfa)(CH$_3$)(CO)(PPh$_3$)(I)], which is an alkyl2 product according to Scheme 1.[32] Knowledge of the stereochemistry of the reaction products may contribute to the rationalization of experimental results and furnish ideas which might be used to design new and better ligands. In this paper, we present a DFT study on the ground state of the molecular structures of the reactants and products of the oxidative addition reaction of the rhodium(I) carbonyl phosphine complex [Rh(fctfa)(CO)(PPh$_3$)] with CH$_3$I, to predict the stereochemistry of possible intermediates during the oxidative addition reaction according to Scheme 1. Results are complemented by a NMR study.

2. Experimental

2.1. Synthesis

[Rh(fctfa)(CO)(PPh$_3$)][36] and [Rh(fctfa)(CH$_3$)(CO)(PPh$_3$)(I)][32] were prepared according to the literature.

2.2. Spectroscopy

NMR measurements at 298 K were recorded on a Bruker Avance II 600 NMR spectrometer [^{1}H (600.130 MHz)]. The chemical shifts were reported relative to SiMe$_4$ (δ = 0.00 ppm). Positive values indicate downfield shift. IR spectra were recorded from neat samples on a Digilab FTS 2000 infrared spectrophotometer utilizing a He-Ne laser at 632.6 nm.

2.3. Quantum Computational Methods

The pure Density Functional Theory (DFT) calculations were carried out using the Amsterdam Density Functional 2006 (ADF) program system[37] with the PW91 (Perdew-Wang, 1991) exchange and correlation functional.[38] As a check on the performance of the PW91 functional, the OLYP[39,43] (OPTX exchange functional[39] combined with the Lee-Yang-Parr correlation functional[40]), the BLYP (Becke's gradient-corrected exchange functional[41] with the Lee-Yang-Parr gradient-corrected correlation functional[40]), the BP86[41,42] and the OPBE[43] Generalized Gradient Approximation (GGA) were also used for selected geometry optimizations. The TZP (triple ζ polarized) basis set, a fine mesh for numerical integration (5.5 for geometry optimizations and 6.0 for frequency calculations), a spin-unrestricted (gas-phase) formalism and full geometry optimization with tight convergence criteria as implemented in the ADF 2006 program, were used unless a different basis set (double-ζ (DZ), double-ζ with polarization functions (DZP), triple-ζ with polarization functions (TZP), triple-ζ with two polarization functions (TZ2P) and quadruple-ζ with four polarization functions (QZ4P) or ZORA[44]) was indicated. Calculations in solution, as contrasted with the gas phase, were done using the Conductor-like Screening Model (COSMO)[45–47] of solvation as implemented in ADF.[48] Hybrid DFT calculations were carried out using the Gaussian-03 program package.[49] The B3LYP[50] (B3 Becke 3-parameter exchange and Lee-Yang-Parr correlation) functional for both exchange and correlation, with the CEP-31G[51] (Stevens/Barch/Krauss effective core potential triple-split) basis set was used.

The accuracy of the different computational approaches was evaluated by comparing the root-mean-square deviations (RMSDs) between the optimized molecular structure and the crystal structure, using the non-hydrogen atoms in the molecule. RMSD values were calculated using the 'RMS Compare Structures' utility in ChemCraft Version 1.5.[52] No symmetry limitations were imposed on the calculations. The standard deviation from experimental values of the calculated metal-ligand bond lengths, *d,* was quantified by calculating the standard deviation of the rhodium-ligand (Rh-L) bond lengths by

$$\sqrt{\frac{(\Delta d_{\text{Rh-O1}})^2 + (\Delta d_{\text{Rh-O2}})^2 + (\Delta d_{\text{Rh-C4}})^2 + (\Delta d_{\text{Rh-P}})^2}{3}} \quad (1)$$

where $\Delta d_{\text{Rh-L}} = d_{\text{Rh-L}}$ (experimental) – $d_{\text{Rh-L}}$(calculated).[53]

Similarly the standard deviation from experimental values of the calculated metal-ligand bond angles, *a,* was quantified by

$$\sqrt{\frac{(\Delta a_{\text{P-Rh-O1}})^2 + (\Delta a_{\text{O1-Rh-O2}})^2 + (\Delta a_{\text{O2-Rh-C4}})^2 + (\Delta a_{\text{C4-Rh-P}})^2}{3}} \quad (2)$$

where $\Delta a_{\text{L-Rh-L'}} = a_{\text{L-Rh-L'}}$ (experimental) – $a_{\text{L-Rh-L'}}$ (calculated).

3. Results and Discussion

Two structural isomers have previously been identified for [Rh(fctfa)(CO)(PPh_3)].[32,54] Mathematically calculated, the different arrangements of the groups bonded to the rhodium(III) centre, after oxidative addition of CH_3I to [Rh(fctfa)(CO)(PPh_3)], give rise to a theoretical possibility of 24 different octahedral Rh^{III}-alkyl isomers and twelve different square pyramidal Rh^{III}-acyl isomers. Since the enantiomers (twelve Rh^{III}-alkyl and six Rh^{III}-acyl mirror images) display the same computational and chemical properties, they can be excluded from this discussion. The twelve different Rh^{III}-alkyl isomers and six different Rh^{III}-acyl isomers are illustrated schematically in Table 1. Only four different Rh^{III}-alkyl isomers and four different Rh^{III}-acyl isomers are experimentally observed according to Scheme 1.[32]

3.1. Spectroscopic Properties of the Rhodium Complexes

In $CDCl_3$ at 25 °C, the signals of the methine proton of the β-diketonato ligand of the different [Rh(fctfa)(CH_3)(CO)(PPh_3)(I)]-alkyl reaction products are presented as singlets at δ 6.10 ppm (alkyl1 isomers overlap) and at δ 5.50 and 5.35 ppm (alkyl2 isomers). The corresponding signals of the [Rh(fctfa)(CO)(PPh_3)] isomers are at δ 6.08 and 6.09 ppm (see Fig. 3).[32] Both [Rh(fctfa)(CO)(PPh_3)][36] and [Rh(fctfa)(CH_3)(CO)(PPh_3)(I)]-alkyl2[32] have been characterized crystallographically. In the crystal structure of [Rh(fctfa)(CH_3)(CO)(PPh_3)(I)]-alkyl2 the PPh_3 group and iodide are above and below the square plane formed by the two oxygens of the β-diketonato ligand and the other two groups bonded to the rhodium centre. The positioning of the PPh_3 group above (or below) the plane as in Rh-alkyl2, implies that as the PPh_3 group rotates, a Ph group will be rotating directly above the methine H of the β-diketonato ligand (see Fig. 3 right). The ring current inside the phenyl ring shields the methine H directly below it to higher field.[55] Thus, the observed shift of the methine proton of the β-diketonato ligand from δ ~6.0 ppm for Rh^{I} to higher field at δ ~5.4 ppm for Rh^{III}-alkyl2 is consistent with the PPh_3 group being positioned above (or below) the plane. By the same reasoning, it is thus expected that the PPh_3 group of the [Rh(fctfa)(CH_3)(CO)(PPh_3)(I)]-alkyl1 isomers in Scheme 1 should be positioned in the square plane formed by the β-diketonato ligand and the other two groups bonded to the rhodium centre. The structures of alkyl III, IV, VII, VIII, XI and XII in Table 1 are thus less likely for alkyl1.

A reaction mixture containing Rh(fctfa)(CH_3)(CO)(PPh_3)(I)]-alkyl1 was cooled down to –15 °C where the reaction was found to be static. A ^1H-^1H NOESY spectrum (see Fig. 4) was recorded at –15 °C to establish the relative dispositions of the CH_3 ligand in the Rh(fctfa)(CH_3)(CO)(PPh_3)(I)]-alkyl1 isomers. Irradiation of the CH_3 resonance on the Rh^{III}-alkyl1 isomers (δ 1.47 and 1.42 ppm), resulted in an NOE coupling with the phenyl (PPh_3) protons. This result is only possible if the CH_3 group of the Rh^{III}-alkyl1 isomers were *cis* to the PPh_3 group, thus excluding alkyl VII and VIII in Table 1 as possible structures for alkyl1 in Scheme 1.

3.2. Computational Results

3.2.1. *Geometrical Study of the Square Planar [Rh(fctfa)(CO)(PPh_3)] Complex*

Since quantum computational methods are applied for the first time to ferrocene-containing rhodium carbonyl phosphine complexes as reported here, some measure of the reliability of the approach had to be obtained. This was addressed by comparing the known single crystal X-ray diffraction structure

Table 1 PW91/TZP relative molecular energies (kJ mol^{-1}) of the possible alkyl and acyl reaction products of the oxidative addition reaction of [Rh(fctfa)(CO)(PPh_3)] and CH_3I in gas phase and in methanol, described by the COSMO model.

β-diketonato	Geometry	Vacuum	CH_3OH solution
alkyl I	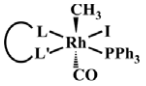	79	–
alkyl II	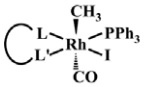	62	–
alkyl III	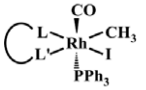	59	–
alkyl IV	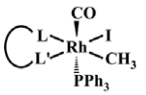	56	–
alkyl V	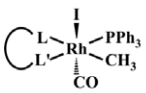	51	–
alkyl VI	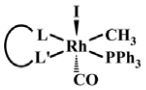	47	–
alkyl VII	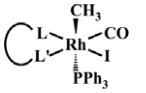	40	50
alkyl VIII	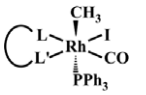	39	47
alkyl IX [a]	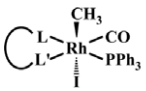	36	35
alkyl X [a]	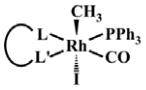	29	29
alkyl XI [b]	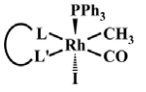	27	29
alkyl XII [b]	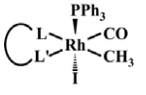	24	26
acyl I	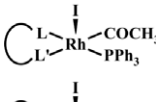	80	–
acyl II	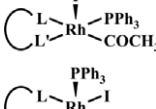	61	–
acyl III	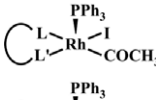	46	42
acyl IV	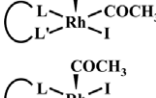	33	33
acyl V [c]	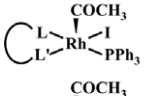	6	6
acyl VI [c]	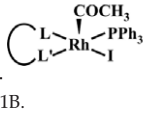	0	0

[a] Alkyl1A and alkyl1B.
[b] Alkyl2A and alkyl2B.
[c] Acyl2A and acyl2B.

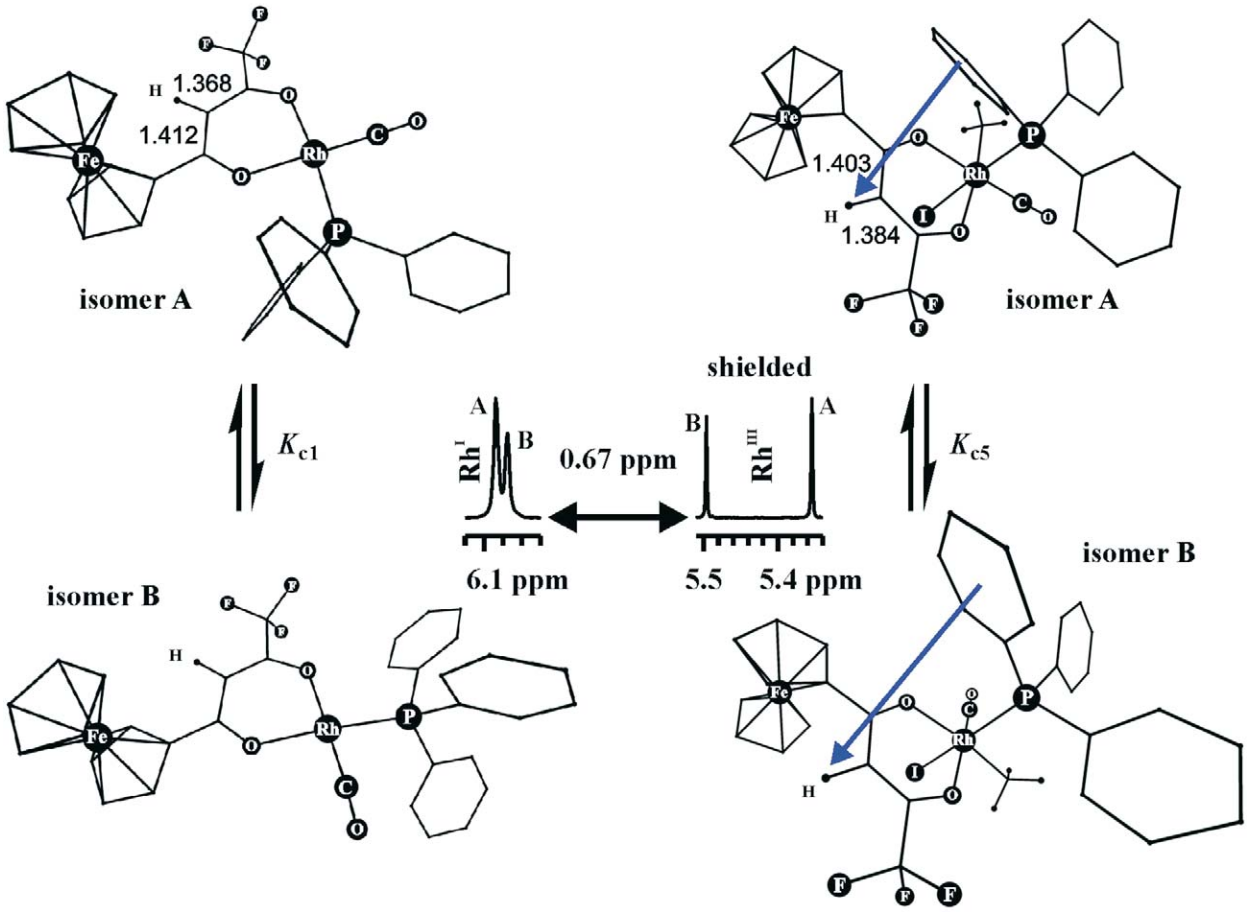

Figure 3 Structure of [Rh(fctfa)(CO)(PPh_3)] (left) and of [Rh(fctfa)(CH_3)(CO)(PPh_3)(I)]-alkyl2 (right), illustrating the shielding effect of the phenyl ring on the methyl proton in alkyl2 resulting in an upfield shift. Two isomers of each are observed. Isomers A are crystal structures and isomers B are calculated structures. Middle: The methine region of the ^{1}H NMR spectrum of [Rh(fctfa)(CO)(PPh_3)] and [Rh(fctfa)(CH_3)(CO)(PPh_3)(I)]-alkyl2.

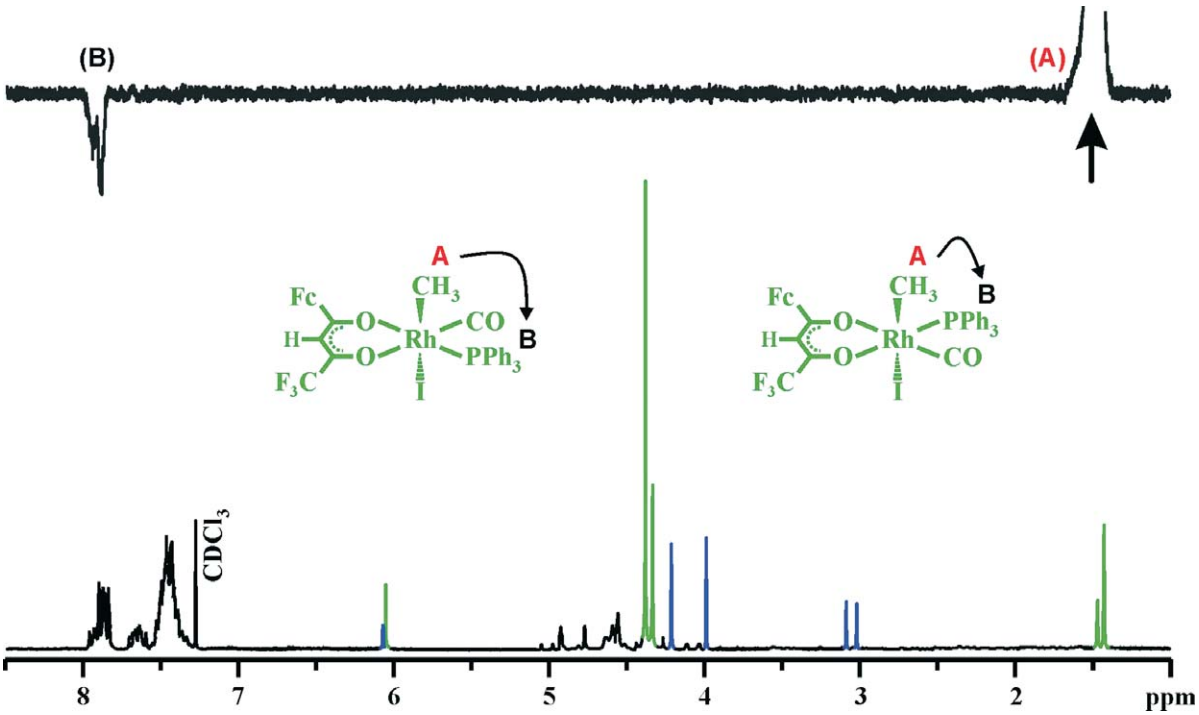

Figure 4 ^{1}H NMR spectrum (bottom) of the reaction mixture (CH_3I suppressed) containing the two [Rh(fctfa)(CH_3)(CO)(PPh_3)(I)]-alkyl1 isomers (green) and the two [Rh(fctfa)($COCH_3$)(PPh_3)(I)]-acyl1 isomers (blue). The NOE spectrum (top) results from irradiation of the methyl groups of the alkyl1 isomers at *ca.* 1.5 ppm at –15 °C, where the reaction was found to be static. The NOE interactions are as indicated with the proposed alkyl1 structure as indicated.

Table 2 The comparison of calculated bond lengths (Å) and bond angles (degree) in [Rh(fctfa)(CO)(PPh_3)], calculated by using different functionals, with the experimental data. For all calculations the TZP basis set was used, except for the B3LYP functional where the CEP-31G basis set was used. The atom numbering is as indicated in Fig. 5.

Bond, angle	Exp.	PW91	BLYP	BP86	OLYP	OPBE	B3LYP
C1-C2	1.412	1.419	1.426	1.420	1.425	1.419	1.440
C2-C3	1.386	1.388	1.393	1.389	1.391	1.386	1.411
C1-O1	1.267	1.286	1.293	1.289	1.281	1.275	1.319
C3-O2	1.264	1.278	1.284	1.280	1.273	1.269	1.309
O1-Rh	2.048	2.093	2.118	2.096	2.115	2.102	2.072
O2-Rh	2.070	2.113	2.139	2.112	2.155	2.125	2.077
P-Rh	2.233	2.228	2.330	2.292	2.309	2.268	2.384
C4-Rh	1.801	1.849	1.872	1.853	1.834	1.813	1.846
C1-C2-C3	124.30	125.4	125.7	125.5	125.3	125.1	123.6
O1-Rh-O2	88.63	89.7	89.0	89.9	87.8	88.4	88.6
O2-Rh-C4	92.94	91.2	90.7	90.1	90.5	90.1	91.1
P-Rh-C4	92.74	92.9	93.8	93.2	92.5	91.5	94.3
P-Rh-O1	85.89	86.4	86.7	87.0	89.4	90.2	86.0
RMSD [a]	–	0.12	0.17	0.16	0.19	0.20	0.50
Standard deviation, Rh-L bond lengths [b]	–	0.045	0.090	0.058	0.079	0.049	0.092
Standard deviation, L-Rh-L′ bond angles [c]	–	1.208	1.555	1.930	2.490	3.086	1.386

[a] RMS values, in Å, are root mean square atom positional deviations, calculated for non-hydrogen atoms for the best three-dimensional superposition of calculated structures on experimental structures.
[b] Calculated by Equation 1.
[c] Calculated by Equation 2.

of [Rh(fctfa)(CO)(PPh_3)][36] with the theoretically calculated structures of the same complex obtained by using a collection of functionals and basis sets (Tables 2 and 3, with the atom numbering as indicated in Fig. 5). A key indicator of structure in organometallic compounds is the bond lengths and angles involving the metal centre. The accuracy of the different calculations was thus evaluated by the standard deviation of the calculated rhodium-ligand bond lengths and angles from experiment

Table 3 Influence of the basis set effect, using the PW91 functional (last two rows OLYP for comparison), on the computed geometrical data of [Rh(fctfa)(CO)(PPh_3)]. The atom numbering is as indicated in Fig. 5.

	–	–	ZORA				RELATIVISTIC/ZORA			
Bond, angle	Exp.	TZP	DZ	TZP	TZ2P	QZ4P	DZ	TZP	TZ2P	QZ4P
C1-C2	1.412	1.419	1.418	1.418	1.417	1.419	1.418	1.417	1.418	1.418
C2-C3	1.386	1.388	1.384	1.387	1.387	1.388	1.384	1.386	1.384	1.384
C1-O1	1.267	1.286	1.317	1.287	1.283	1.283	1.319	1.289	1.319	1.319
C3-O2	1.264	1.278	1.313	1.278	1.275	1.275	1.316	1.280	1.316	1.316
O1-Rh	2.048	2.093	2.083	2.094	2.085	2.089	2.062	2.071	2.062	2.062
O2-Rh	2.070	2.113	2.096	2.116	2.108	2.097	2.068	2.088	2.068	2.068
P-Rh	2.233	2.228	2.364	2.288	2.270	2.284	2.341	2.262	2.341	2.341
C4-Rh	1.801	1.849	1.863	1.852	1.839	1.832	1.839	1.829	1.839	1.839
C1-C2-C3	124.3	125.4	125.8	125.5	125.1	125.2	125.4	125.1	125.4	125.4
O1-Rh-O2	88.6	89.7	90.4	89.6	88.9	89.2	90.7	90.0	90.7	90.7
O2-Rh-C4	92.9	91.2	91.8	91.6	92.4	91.6	91.4	90.6	91.4	91.4
P-Rh-C4	92.7	92.9	94.3	93.4	92.7	92.1	94.3	93.2	94.3	94.3
P-Rh-O1	85.9	86.4	83.8	85.6	86.3	87.3	83.8	86.4	83.8	83.8
RMSD (PW91 data) [a]	–	0.12	0.12	0.10	0.09	0.13	0.12	0.15	0.12	0.12
Standard deviation, Rh-L bond lengths (PW91 data) [b]	–	0.045	0.087	0.057	0.043	0.045	0.067	0.029	0.067	0.067
Standard deviation, L-Rh-L′ bond angles (PW91 data) [c]	–	1.208	1.930	1.015	0.432	1.241	2.090	1.586	2.090	2.090
RMSD (OLYP data) [a]	–	0.19	0.18	0.16	–	0.25	0.18	0.22	0.21	0.26
Standard deviation, Rh-L bond lengths (OLYP data) [b]	–	0.079	0.107	0.083	–	0.072	0.078	0.050	0.040	0.038
Standard deviation, L-Rh-L′ bond angles (OLYP data) [c]	–	2.490	1.803	1.828	–	3.698	2.160	3.968	2.826	3.572

[a] RMS values, in Å, are root mean square atom positional deviations, calculated for non-hydrogen atoms for the best three-dimensional superposition of calculated structures on experimental structures.
[b] Calculated by Equation 1.
[c] Calculated by Equation 2.

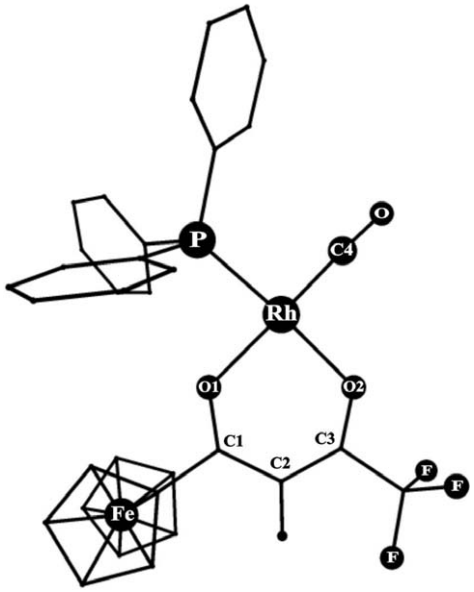

Figure 5 The structure of [Rh(fctfa)(CO)(PPh_3)], indicating the numbering system as used in Tables 2 and 3.

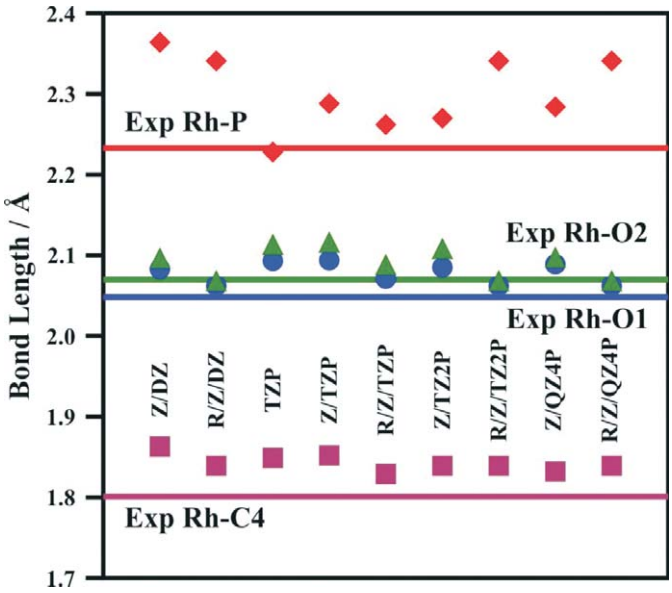

Figure 6 Computed bond lengths (Å) of [Rh(fctfa)(CO)(PPh_3)] as a function of the applied basis set using the PW91 functional. Z = ZORA basis set, R = relativistic calculation.

(Equations 1 and 2), while the root-mean-square (RMS) distances between the theoretical and the experimental structures give an account of the overall accuracy of the calculated results.

3.2.1.1. *Influence of the Functional Form*

In Table 2, the structural data for [Rh(fctfa)(CO)(PPh_3)], using a variety of different functional forms, are listed. All functionals succeed in reproducing the experimental bond lengths within 0.1 Å, except for the B3LYP calculated Rh-P bond, which is 0.15 Å too long. Focussing on both the RMS distances of all the non-hydrogen bonds in combination with the standard deviations of the rhodium-ligand bond lengths and angles, as quantified by Equations 1 and 2, the pure classical PW91 outperformed the other functionals with the hybrid functional B3LYP performing the worst. The PW91 functional was thus used in further calculations.

3.2.1.2. *Basis Set Effects*

The effect of the basis set was determined by using the PW91 functional, as well as OLYP for comparison, for a variety of basis sets. When increasing the basis set size from DZ to QZ4P (Table 3), a slight improvement was observed for PW91. The ZORA basis set did not perform better when going from DZ to TZ2P, QZ4P. Relativistic calculations with the ZORA approach did not perform better than TZP. Gas phase calculations generally give longer bond lengths than corresponding solid state crystal structure bond lengths.[56] All the calculated gas phase bond lengths, in particular the Rh-ligand bond lengths, were found to be slightly longer than the corresponding solid state bond lengths from crystal data (see Fig. 6). The largest deviation from experimental bond lengths was found for the P-Rh bond, except for the PW91/TZP calculation. The PW91 functional with the TZP basis set was used in all further calculations.

3.2.1.3. *PW91/TZP Results of the [Rh(fctfa)(CO)(PPh_3)] Isomers*

The PW91/TZP calculated minimum energy geometries of the square-planar rhodium(I) [Rh(fctfa)(CO)(PPh_3)] isomers A (geometry known by X-ray crystallography) and B are reported in Fig. 7. In agreement with X-ray data, the experimental Rh-L bond lengths of isomer A are reproduced with an accuracy of 0.02 Å for Rh-O, 0.05 Å for Rh-C and 0.005 Å for Rh-P. Calculated bond lengths between atoms inside the fctfa ligand fit the measured values generally within the range of 0.01 Å. The angles involving Rh deviate 0.2 to 1.7 ° from the experimental values. Since comparisons of experimental metal-ligand bond lengths with calculated bond lengths below a threshold of 0.02 Å are considered as meaningless,[56] structural data computed with the PW91/TZP model for related compounds may be presented with an extrapolative equally high degree of accuracy.

The larger *trans* influence of the PPh_3 group, relative to the CO group, is well reproduced by the elongated Rh-O bond *trans* to the PPh_3 group. The calculated Rh-P bond lengths of 2.288 and 2.303 Å for isomers A and B, respectively, are within the typical range of Rh-P distances of 2.232–2.252 Å for related [Rh^{I}(β-diketonato)(CO)(PPh_3)] complexes.[57–62] The calculated Rh-C bond lengths (1.849 and 1.845 Å for isomers A and B, respectively) are slightly longer (0.03 Å) than the Rh-C bond lengths (1.739–1.813 Å) in related experimental structures.[58–62]

3.2.2. *IR Carbonyl Stretching Frequency (ν_{CO}) Study of Ferrocenoyltrifluoroacetonato-containing Rhodium(I) Complexes*

The dicarbonyl rhodium(I) complexes [Rh^{I}(β-diketonato)($CO)_2$], give an IR spectrum with two distinctive singlet ν_{CO} peaks – one for the symmetric and one for the antisymmetric carbonyl stretching. Replacement of one of these CO groups with a PPh_3 group results in a monocarbonyl phosphine [Rh^{I}(β-diketonato)(CO)(PPh_3)] complex. Consequently only one ν_{CO} peak for each isomer of [Rh^{I}(β-diketonato)(CO)(PPh_3)] was observed, represented by the one CO group. Frequency calculations were preformed on the optimized structures to obtain the carbonyl stretching frequencies (ν_{CO}). The calculated and experimental carbonyl stretching frequency data of [Rh(fctfa)($CO)_2$], [Rh(fctfa)(CO)(PPh_3)] and [Rh(fctfa)(CH_3)(CO)(PPh_3)(I)]-alkyl2, as illustrated graphically in Fig. 8, yielded unscaled calculated ν_{CO} values in excellent agreement with the experimentally obtained values.

3.2.3. *Rhodium(III) Oxidative Addition Products*

The calculated relative molecular energies of the twelve possible octahedral Rh^{III}-alkyl and six possible square-pyramidal

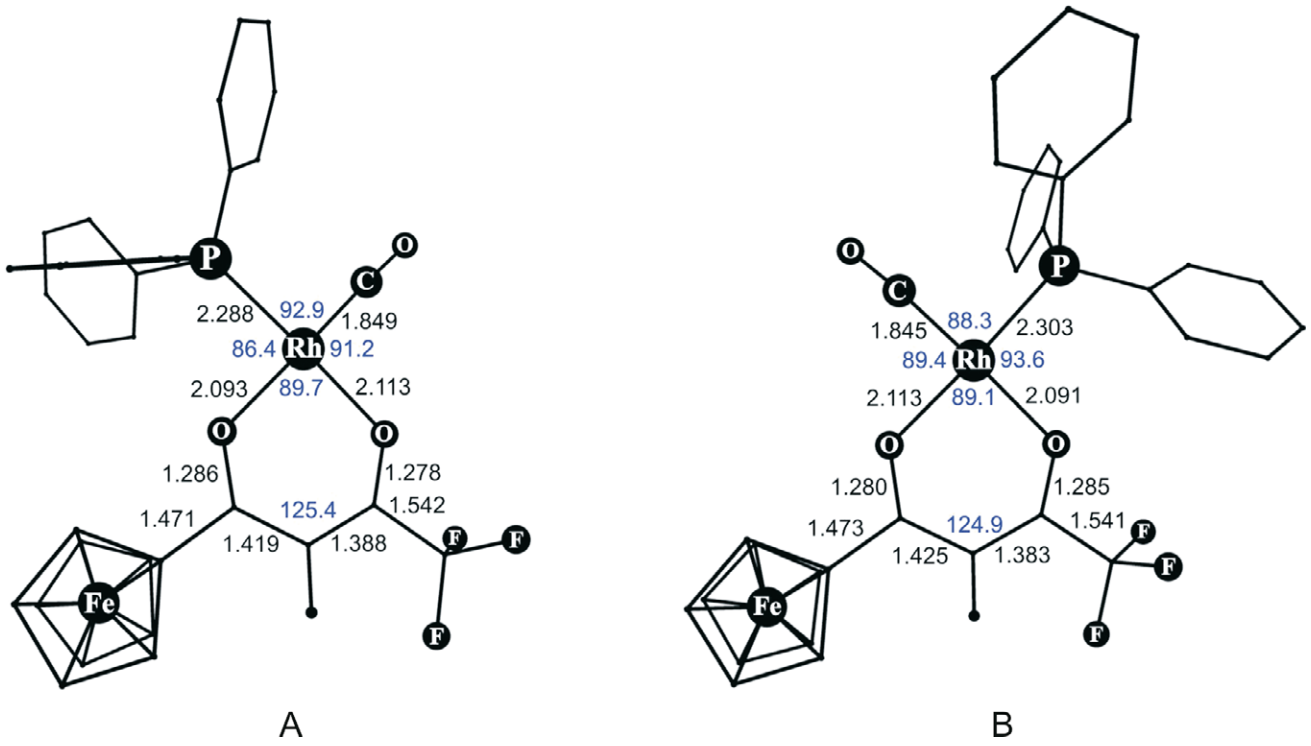

Figure 7 The PW91/TZP calculated minimum energy geometries of the square-planar rhodium(I) [Rh(fctfa)(CO)(PPh_3)] isomers A (left) and B (right) before CH_3I addition. The crystal structure of isomer A (left) was solved by X-ray crystallography. Bond lengths (Å, black) and bond angles (degree, blue) are as indicated.

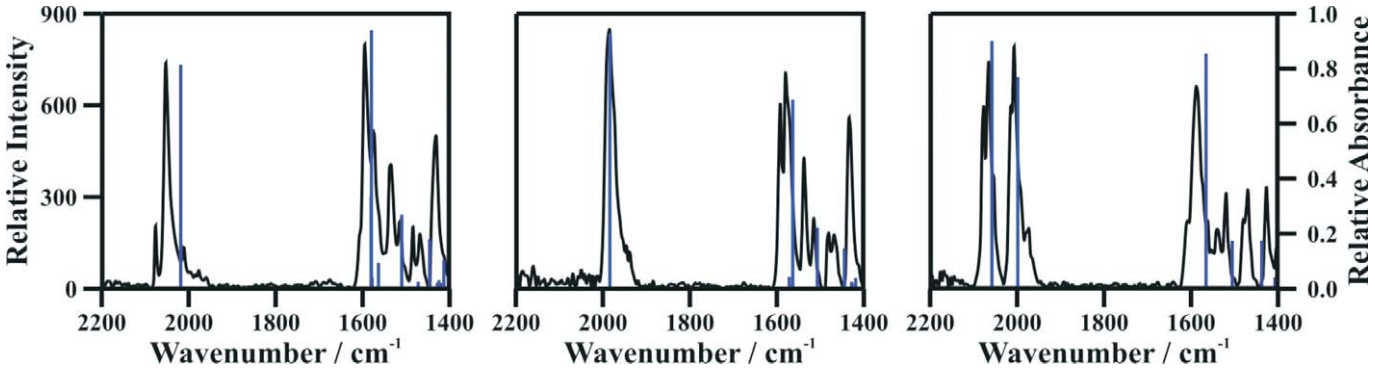

Figure 8 Experimental (black curves) and PW91/TZP calculated (blue bars) IR spectra of [Rh(fctfa)($CO)_2$] (left), [Rh(fctfa)(CO)(PPh_3)] isomer A (middle) and [Rh(fctfa)(CH_3)(CO)(PPh_3)(I)]-alkyl2A (right).

Rh^{III}-acyl reaction products of [Rh(fctfa)(CO)(PPh_3)] with CH_3I for gas phase calculations, as well as in solution in methanol, are reported in Table 1. Trigonal bipyramidal Rh^{III}-acyl isomers were also considered, but resulted in such high calculated relative molecular energies that they were discarded from this study.

3.2.3.1. *Octahedral Rhodium(III)-alkyl Products*

When comparing the relative energies of the different Rh^{III}-alkyl complexes in Table 1, the lowest energy alkyl isomers are alkyl XI and alkyl XII. The stereo arrangement of the calculated most stable alkyl XII corresponds to the isolated [Rh(fctfa)(CH_3)(CO)(PPh_3)(I)]-alkyl2 reaction product characterized by X-ray crystallography, in Scheme 1. Good agreement exists between the calculated geometry of the most stable Rh^{III}-alkyl complex alkyl XII and the crystal structure of [Rh(fctfa)(CH_3)(CO)(PPh_3)(I)]-alkyl2 (Fig. 9). The acidity of the

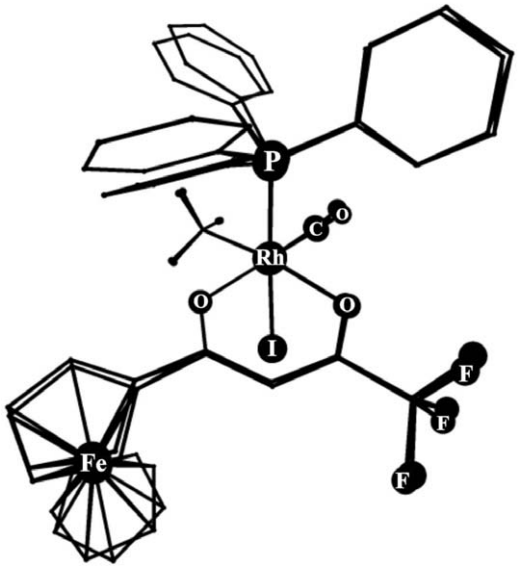

Figure 9 An overlay view of the calculated (alkyl XII) and the experimental X-ray determined structure of [Rh(fctfa)(CH_3)(CO)(PPh_3)(I)]-alkyl2A.

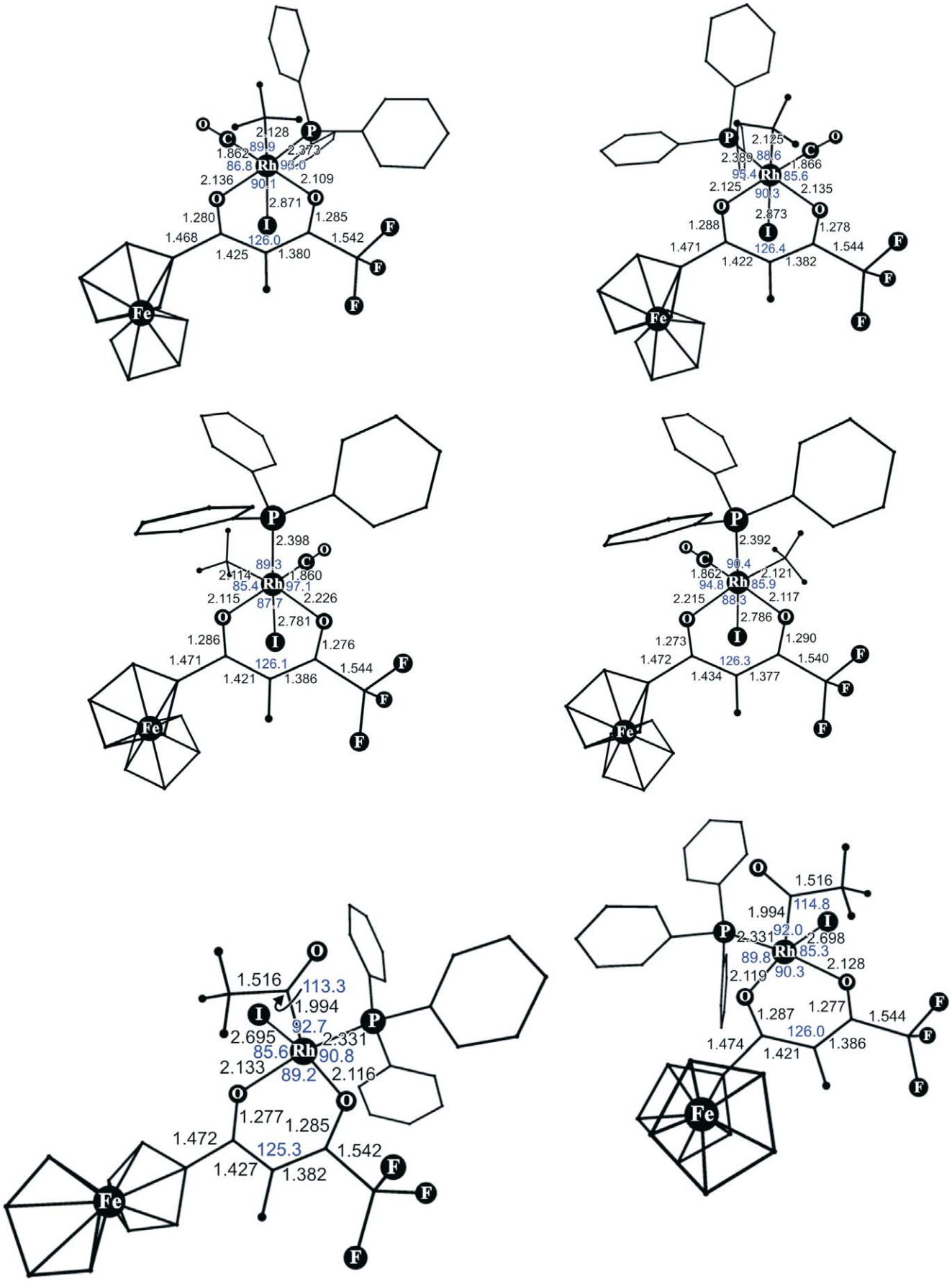

Figure 10 The PW91/TZP calculated minimum energy geometries of the octahedral [Rh(fctfa)(CH_3)(CO)(PPh_3)(I)]-alkyl complexes after *trans* CH_3I addition (top), the octahedral [Rh(fctfa)(CH_3)(CO)(PPh_3)(I)]-alkyl complexes with the PPh_3 group and I above and below the square plane (middle) and the square-pyramidal [Rh(fctfa)($COCH_3$)(PPh_3)(I)]-acyl products after CO insertion (bottom). Bond lengths (Å, black) and bond angles (degree, blue) are as indicated.

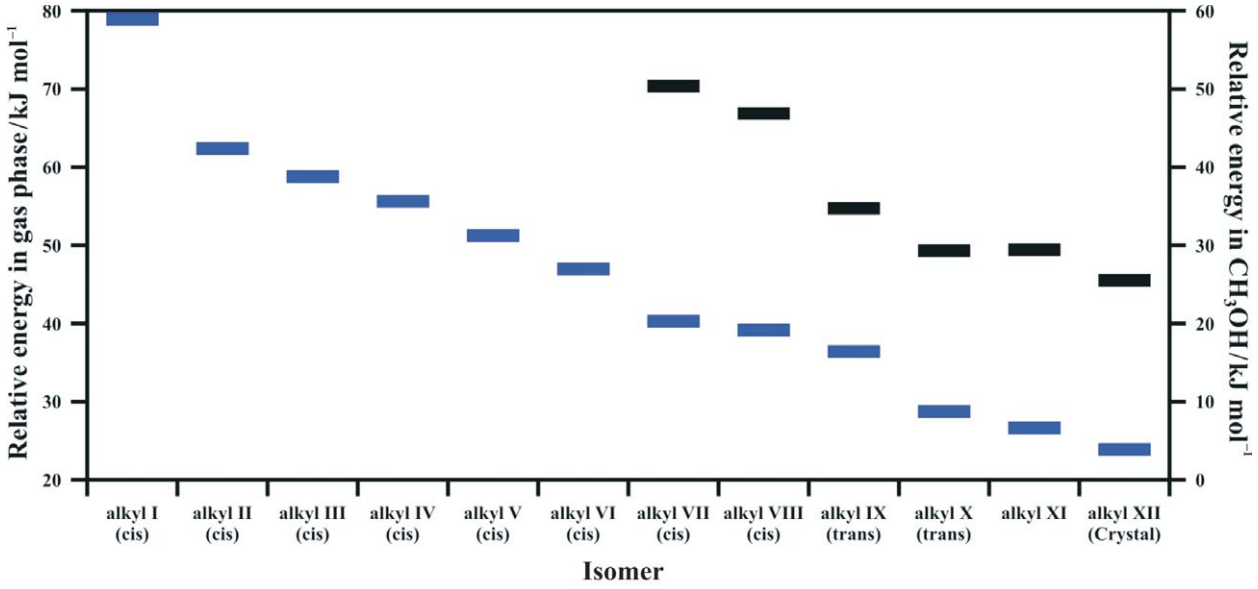

Figure 11 The PW91/TZP calculated relative energies (kJ mol^{-1}) of the octahedral [Rh(fctfa)(CH_3)(CO)(PPh_3)(I)]-alkyl complexes in gas phase (blue) and in CH_3OH solution (black).

Ph-substituted phosphorus reduces the electron density at the rhodium atom and hence stabilizes the *trans* π-electron donating ligand I^-, resulting in the calculated Rh-I bond lengths *trans* to PPh_3 (Fig. 10 middle) being *ca.* 0.01 Å shorter than the Rh-I bond lengths *trans* to CH_3 (Fig. 10 top).

In determining the geometry of the alkyl1 isomers in Scheme 1, one can discard the upper six Rh^{III}-alkyl isomers in Table 1, since they are not energetically favoured. CH_3I will either be added *cis* or *trans* to the square planar Rh^I complex. The lowest energy *cis* addition products are alkyl VII and alkyl VIII (unlikely on grounds of ^1H NOESY results, Fig. 4), while the *trans* addition products are alkyl IX and alkyl X (Fig. 11). Gas phase calculations did not favour the *trans* addition products by a clear margin of energy. In order to fulfil experimental conditions, calculations taking solvent effects into account were also performed. In methanol the *trans* addition products, alkyl IX and alkyl X, are favoured by *ca.* 15 kJ mol^{-1} over the *cis* addition products alkyl VII and alkyl VIII. These results are consistent with alkyl IX and alkyl X corresponding to the alkyl1 isomers of Scheme 1, suggesting a *trans* addition of CH_3I to [Rh(fctfa)(CO)(PPh_3)]. The [Rh(fctfa)(CH_3)(CO)(PPh_3)(I)]-alkyl2 isomers result from isomerization of the *trans* addition product (alkyl IX and alkyl X) *via* an acyl to the thermodynamically more stable *cis* alkyl addition product (alkyl XI and alkyl XII).

The stereochemistry of the alkyl1 isomers, alkyl IX and alkyl X (Fig. 10 top), and the stereochemistry of the alkyl2 isomers, alkyl XI and alkyl XII (Fig. 10 middle), correspond with the stereochemistry of Class 1 and Class 2 crystals, respectively, as described in the introduction. Thus computational, NMR and crystal structure results are mutually consistent with the alkyl1 isomers having the CH_3 group and the iodide above and below the square plane and the alkyl2 isomers having the PPh_3 group and the iodide above and below the square plane of the octahedral Rh^{III}-alkyl reaction products.

3.2. Square-pyramidal Rhodium(III)-acyl Products

The most stable products of the different Rh^{III}-acyl complexes in Table 1 are clearly the acyl V and acyl VI isomers, with the $COCH_3$ moiety in the apical position as illustrated in Fig. 10 bottom. This geometry correlates with the geometry of the Class 3 crystal structures of the [Rh^{III}(L,L'-BID)($COCH_3$)(PPh_3)(I)] class of compounds as described in the introduction. Thus, both computational calculations and crystallography are consistent with the geometry of the thermodynamically stable reaction product, the acyl2 isomers in Scheme 1, being square-pyramidal with the $COCH_3$ group in the apical position.

The calculated Rh-P bond lengths of the Rh^{III}-acyl complexes are longer (2.33 Å versus 2.30 Å) than the calculated Rh-P bond lengths in the parent rhodium(I) complexes, indicating that a change in oxidation state from rhodium(I) to rhodium(III) results in a weaker Rh-P bond. The calculated Rh-P (2.331 Å) and Rh-C (1.994 Å) bond lengths fall well inside the range of experimental bond lengths in related Rh^{III}-acyl complexes (2.254–2.341 Å and 1.956–2.005 Å, respectively).[28–30,63]

4. Conclusions

DFT calculations, in agreement with crystal data, gave a solid account of the geometry of [Rh(fctfa)(CO)(PPh_3)]. NMR, crystal structure and computational chemistry results on the stereochemistry of the Rh^{III}-alkyl1, Rh^{III}-alkyl2 and Rh^{III}-acyl2 reaction products, as given by Scheme 1, are mutually consistent with the conclusion that (i) the alkyl1 product results from *trans* addition to Rh^I, (ii) that the thermodynamic alkyl2 product adopts an octahedral geometry with the PPh_3 group and the iodide above and below the square plane formed by the two oxygens of the β-diketonato ligands and the other two groups bonded to the rhodium centre, and (iii) that the thermodynamic acyl product adopts a square-pyramidal geometry with the $COCH_3$ group in the apical position.

Supplementary Material

A summary of the optimized Cartesian coordinates of the studied molecules is provided in the supplementary material.

Acknowledgements

Financial assistance by the South African National Research Foundation, under grant number 2067416, and the Central Research Fund of the University of the Free State is gratefully acknowledged.

References

1 D. Forster, *J. Am. Chem. Soc.*, 1976, **98**, 846–848.
2 D. Forster, *Adv. Organomet. Chem.*, 1979, **17**, 255–267.

3 P.M. Maitlis, A. Haynes, G.J. Sunley and M.J. Howard, *J. Chem. Soc., Dalton Trans.,* 1996, 2187–2196.

4 A. Haynes, B.E. Mann, G.E. Morris and P.M. Maitlis, *J. Am. Chem. Soc.,* 1993, **115**, 4093–4100.

5 L. Gonsalvi, H. Adams, G.J. Sunley, E. Ditzel and A. Haynes, *J. Am. Chem. Soc.,* 1999, **121**, 11233–11234.

6 T.R. Griffin, D.B. Cook, A. Haynes, J.M. Pearson, D. Monti and G.E. Morris, *J. Am. Chem. Soc.,* 1996, **118**, 3029–3030.

7 S.B. Dake and R.V. Chaudhari, *J. Mol. Catal.,* 1984, **26**, 135–138.

8 M. Cheong, R. Schmid and T. Ziegler, *Organometallics,* 2000, **19**, 1973–1982.

9 T. Kinnunen and K. Laasonen, *J. Mol. Struct. (Theochem),* 2001, **540**, 91–100.

10 E.A. Ivanova, P. Gisdakis, V.A. Nasluzov, A.U. Rubailo and N. Rösch, *Organometallics,* 2001, **20**, 1161–1174.

11 S.S. Basson, J.G. Leipoldt and J.T. Nel, *Inorg. Chim. Acta,* 1984, **84**, 167–172.

12 S.S. Basson, J.G. Leipoldt, A. Roodt, J.A. Venter and T.J. van der Walt, *Inorg. Chim. Acta,* 1986, **119**, 35–38.

13 J.G. Leipoldt, S.S. Basson and L.J. Botha, *Inorg. Chim. Acta,* 1990, **168**, 215–220.

14 J.A. Venter, J.G. Leipoldt and R. van Eldik, *Inorg. Chem.,* 1991, **30**, 2207–2209.

15 G.J.J. Steyn, A. Roodt and J.G. Leipoldt, *Inorg. Chem.,* 1992, **31**, 3477–3481.

16 G.J.J. Steyn, A. Roodt and J.G. Leipoldt, *Rhodium Ex.,* 1993, **1**, 25–29.

17 A. Roodt and G.J.J. Steyn, *Recent Res. Devel. Inorganic Chem.,* 2000, **2**, 1–23.

18 E.P. Shestakova, T.G. Cherkasova, L.V. Osetrova, Y.S. Varshavsky, A. Roodt and J.G. Leipoldt, *Rhodium Ex.,* 1994, **7**, 30–38.

19 G.J. Lamprecht and J.H. Beetge, *S. Afr. J. Chem.,* 1987, **40**, 131–133.

20 G.J. van Zyl, G.J. Lamprecht and J.G. Leipoldt, *Inorg. Chim. Acta,* 1986, **122**, 75–79.

21 G.J. van Zyl, G.J. Lamprecht, J.G. Leipoldt and T.W. Swaddle, *Inorg. Chim. Acta,* 1988, **143**, 223–227.

22 K.G. van Aswegen, J.G. Leipoldt, I.M. Potgieter, G.J. Lamprecht, A. Roodt and G.J. van Zyl, *Transition Met. Chem.,* 1991, **16**, 369–371.

23 P. Braunstein, Y. Chauvin, J. Fischer, H. Olivier, C. Strohmann and D.V. Toronto, *New J. Chem. (Nouv. J. Chim.*), 2000, **24**, 437–445.

24 L.J. Damoense, W. Purcell, A. Roodt and J.G. Leipoldt, *Rhodium Ex.,* 1994, **5**, 10–13.

25 S.S. Basson, J.G. Leipoldt, A. Roodt and J.A. Venter, *Inorg. Chim. Acta,* 1987, **128**, 31–37.

26 M. Cano, J.V. Heras, M.A. Lobo, E. Pinilla and M.A. Monge, *Polyhedron,* 1992, **11**, 2679–2690.

27 J.A. Venter, S.S. Basson and W. Purcell, manuscript in preparation.

28 J.A. Cabeza, V. Riera, M.A. Villa-Garcia, L. Ouahab and S. Triki, *J. Organomet. Chem.*, 1992, **441**, 323–331.

29 C.H. Cheng, B.D. Spivack and R. Eisenberg, *J. Am. Chem. Soc.,* 1977, **99**, 3003–3011.

30 L.J. Damoense, W. Purcell and A. Roodt, *Rhodium Ex.,* 1995, **14**, 4–10.

31 M.M. Conradie and J. Conradie, article in press: *Inorg. Chim. Acta,* 2008, doi:*10.1016/j.ica.2007.10.052*

32 J. Conradie, G.J. Lamprecht, A. Roodt and J.C. Swarts, *Polyhedron,* 2007, **23**, 5075–5087.

33 Y.S. Varshavsky, T.G. Cherkasova, N.A. Buzina and J. Bresler, *Organomet. Chem.,* 1994, **464**, 239–245.

34 M.M. Conradie and J. Conradie, *Inorg. Chim. Acta*, 2008, **361**, 208–218.

35 Cambridge Structural Database (CSD), Version 5.27, August 2006 update.

36 G.J. Lamprecht, J.C. Swarts, J. Conradie and J.G. Leipoldt, *Acta Cryst.,* 1993, **C49**, 82–84.

37 G.T. Velde, F.M. Bickelhaupt, E.J. Baerends, C.F. Guerra, S.J.A. van Gisbergen, J.G. Snijders and T.J. Ziegler, *J. Comput. Chem.,* 2001, **22**, 931–967.

38 J.P. Perdew, J.A. Chevary, S.H. Vosko, K.A. Jackson, M.R. Perderson, D.J. Singh and C. Fioihais, *Phys. Rev.,* 1992, **B46**, 6671–6687.

39 N.C. Handy and A. Cohen, *Mol. Phys.,* 2001, **99**, 403–412.

40 (a) C. Lee, W. Yang and R.G. Parr, *Phys. Rev.,* 1988, **B37**, 785–789; (b) B. Miehlich, A. Savin, H. Stoll and H. Preuss, *Chem. Phys. Lett.,* 1989, **157**, 200–206.

41 A.D. Becke, *Phys. Rev.,* 1998, **A38**, 3098–3100.

42 J.P. Perdew, *Phys. Rev.,* 1986, **B33**, 8822–8824. Erratum: J.P. Perdew, *Phys. Rev.,* 1986, **B34**, 7406.

43 J.P. Perdew, K. Burke and M. Ernzerhof, *Phys. Rev. Lett.,* 1996, **77**, 3865–3868. Erratum: J.P. Perdew, K. Burke and M. Ernzerhof, *Phys. Rev. Lett.,* 1997, **78**, 1396.

44 E. van Lenthe, A.E. Ehlers and E.J. Baerends, *J. Chem. Phys.,* 1999, **110**, 8943–8953 and references therein.

45 A. Klamt and G. Schüürmann, *J. Chem. Soc., Perkin Trans.,* 1993, **2**, 799–805.

46 A. Klamt, *J. Phys. Chem.,* 1995, **99**, 2224–2235.

47 A. Klamt and V.J. Jones, *J. Chem. Phys.,* 1996, **105**, 9972–9981.

48 C.C. Pye and T. Ziegler, *Theor. Chem. Acc.,* 1999, **101**, 396–408.

49 Gaussian 03, Revision C.02: M.J. Frisch, G.W. Trucks, H.B. Schlegel, G.E. Scuseria, M.A. Robb, J.R. Cheeseman, J.A. Montgomery, jr., T. Vreven, K.N. Kudin, J.C. Burant, J.M. Millam, S.S. Iyengar, J. Tomasi, V. Barone, B. Mennucci, M. Cossi, G. Scalmani, N. Rega, G.A. Petersson, H. Nakatsuji, M. Hada, M. Ehara, K. Toyota, R. Fukuda, J. Hasegawa, M. Ishida, T. Nakajima, Y. Honda, O. Kitao, H. Nakai, M. Klene, X. Li, J.E. Knox, H.P. Hratchian, J.B. Cross, V. Bakken, C. Adamo, J. Jaramillo, R. Gomperts, R.E. Stratmann, O. Yazyev, A.J. Austin, R. Cammi, C. Pomelli, J.W. Ochterski, P.Y. Ayala, K. Morokuma, G.A. Voth, P. Salvador, J.J. Dannenberg, V.G. Zakrzewski, S. Dapprich, A.D. Daniels, M.C. Strain, O. Farkas, D.K. Malick, A.D. Rabuck, K. Raghavachari, J.B. Foresman, J.V. Ortiz, Q. Cui, A.G. Baboul, S. Clifford, J. Cioslowski, B.B. Stefanov, G. Liu, A. Liashenko, P. Piskorz, I. Komaromi, R.L. Martin, D.J. Fox, T. Keith, M.A. Al-Laham, C.Y. Peng, A. Nanayakkara, M. Challacombe, P.M.W. Gill, B. Johnson, W. Chen, M.W. Wong, C. Gonzalez and J.A. Pople, Gaussian Inc., Wallingford, CT, USA, 2004.

50 (a) P.J. Stephens, F.J. Devlin, C.F. Chabalowski and M.J. Frisch, *J. Phys. Chem.,* 1994, **98**, 11623–11627; (b) A. Watson, N.C. Handy and A.J. Cohen, *J. Chem. Phys.,* 2003, **119**, 6475–6491; (c) R.H. Hertwig and W. Koch, *Chem. Phys. Lett.,* 1997, **268**, 345–351.

51 (a) W. Stevens, H. Basch and J. Krauss, *J. Chem. Phys.,* 1984, **81**, 6026–6033; (b) W.J. Stevens, M. Krauss, H. Basch and P.G. Jasien, *Can. J. Chem.*, 1992, **70**, 612–615; (c) T.R. Cundari and W.J. Stevens, *J. Chem. Phys.,* 1993, **98**, 5555–5565.

52 G.A. Zhurko and D.A. Zhurko, Chem Craft, Version 1.5 (build 275), 2007 (www.chemcraftprog.com).

53 D.A. Skoog, D.M. West and F.J. Holler, *Fundamentals of Analytical Chemistry,* 7th edn., Brooks/Cole, Melbourne, Australia, 1996, p. 28.

54 J. Conradie, G.J. Lamprecht, S. Otto and J.C. Swarts, *Inorg. Chim. Acta,* 2002, **328**, 191–203.

55 J. Clayden, N. Greeves, S. Warren and P. Wothers, *Organic Chemistry,* Oxford University Press, Oxford, UK, 2001, p. 251.

56 W.J. Hehre, *A Guide to Molecular Mechanisms and Quantum Chemical Calculations,* Wavefunction Inc., Irvine, CA, USA, 2003, pp. 153,181.

57 J.G. Leipoldt, S.S. Basson and J.T. Nel, *Inorg. Chim. Acta,* 1983, **74**, 85–88.

58 J.G. Leipoldt, S.S. Basson and J.H. Potgieter, *Inorg. Chim. Acta,* 1986, **117**, L3–L5.

59 E.C. Steynberg, G.J. Lamprecht and J.G. Leipoldt, *Inorg. Chim. Acta,* 1987, **133**, 33–37.

60 G.J. Lamprecht, J.C. Swarts, J. Conradie and J.G. Leipoldt, *Acta Crystallogr., Sect. C: Cryst. Struct. Commun.,* 1993, **C49**, 82–84.

61 D. Lamprecht, G.J. Lamprecht, J.M. Botha, K. Umakoshi and Y. Sasaki, *Acta Crystallogr.,* 1997, **C53**, 1403–1405.

62 W. Purcell, S.S. Basson, J.G. Leipoldt, A. Roodt and H. Preston, *Inorg. Chim. Acta,* 1995, **234**, 153–156.

63 G.J.J. Steyn, *Mechanistic study of Nitrogen/Sulphur Donor Atom Bidentate Ligand Influence on the Iodomethane Oxidative Addition to Carbonylphosphinerhodium(I) Complexes,* Ph.D. thesis, University of the Free State, Bloemfontein, South Africa, 1994.